PHYSICAL REVIEW D **94,** 063502 (2016)

Bringing isolated dark matter out of isolation: Late-time reheating and indirect detection

Adrienne L. Erickcek,[1] Kuver Sinha,[2] and Scott Watson[2]

[1]*Department of Physics and Astronomy, University of North Carolina at Chapel Hill, Phillips Hall CB 3255, Chapel Hill, North Carolina 27599, USA*

[2]*Department of Physics, Syracuse University, Syracuse, New York 13244, USA*

(Received 14 October 2015; revised manuscript received 10 July 2016; published 7 September 2016)

In standard cosmology, the growth of structure becomes significant following matter-radiation equality. In nonthermal histories, where an effectively matter-dominated phase occurs due to scalar oscillations prior to big bang nucleosynthesis, a new scale at smaller wavelengths appears in the matter power spectrum. Density perturbations that enter the horizon during the early matter-dominated era (EMDE) grow linearly with the scale factor prior to the onset of radiation domination, which leads to enhanced inhomogeneity on small scales if dark matter (DM) thermally and kinetically decouples during the EMDE. The microhalos that form from these enhanced perturbations significantly boost the self-annihilation rate for dark matter. This has important implications for indirect detection experiments: the larger annihilation rate may result in observable signals from dark matter candidates that are usually deemed untestable. As a proof of principle, we consider binos in heavy supersymmetry with an intermediate extended Higgs sector and all other superpartners decoupled. We find that these isolated binos, which lie under the neutrino floor, can account for the dark matter relic density and decouple from the standard model early enough to preserve the enhanced small-scale inhomogeneity generated during the EMDE. If early forming microhalos survive as subhalos within larger microhalos, the resulting boost to the annihilation rate for bino dark matter near the pseudoscalar resonance exceeds the upper limit established by Fermi-LAT's observations of dwarf spheroidal galaxies. These DM candidates motivate the N-body simulations required to eliminate uncertainties in the microhalos' internal structure by exemplifying how an EMDE can enable Fermi-LAT to probe isolated dark matter.

DOI: 10.1103/PhysRevD.94.063502

I. INTRODUCTION

One missing piece in our reconstruction of the history of the Universe is the period between inflation and the onset of big bang nucleosynthesis (BBN). When computing the dark matter (DM) abundance predicted by a particular extension of the standard model (SM), it is customary to assume that the Universe was radiation dominated long before BBN. However, deviations from radiation domination in the early Universe are required in order to generate the primordial perturbations necessary to seed the growth of large-scale structure, with cosmic inflation providing a compelling explanation. This raises the following question: when did the Universe become radiation dominated? Both prolonged inflationary reheating and the existence of gravitationally coupled scalars (moduli) provide independent motivation that the Universe could have been matter dominated until the time of BBN. In both situations, oscillating scalar fields dominate the energy density of the Universe, leading to an early matter-dominated era (EMDE) prior to BBN [1]. If DM thermally decouples during an EMDE, the relationship between its annihilation cross section and its current abundance radically changes, and particle physics models that predict too much DM in standard thermal histories become viable [2,3].

The impact of an EMDE on the evolution of small-scale structure provides hope of constraining these scenarios [4–6]. The key point is that while matter perturbations only grow logarithmically with the scale factor during radiation domination, they grow linearly during an EMDE. Consequently, perturbations that enter the horizon during the EMDE experience an early stage of linear growth. If DM decouples both thermally and kinetically prior to the onset of radiation domination, this enhancement of the small-scale matter power spectrum leads to the formation of sub-Earth-mass microhalos that contain most of the DM at high redshift. These microhalos are then the building blocks of subsequent structure formation, and their presence in present-day halos enhances the DM annihilation rate by several orders of magnitude. Depending on the outcome of microhalo mergers, this boost to the annihilation rate can be large enough to make these models accessible to gamma-ray observations in spite of the particles' small annihilation cross sections [6].

Demanding that the dark matter thermally and kinetically decouples prior during the EMDE and that its relic abundance matches observations constrains both its annihilation cross section and the strength of its interactions with SM particles. The masses and annihilation cross

sections of DM candidates that can generate observable signals are even more restricted: if the DM particle thermally decouples too long before the Universe becomes radiation dominated, its annihilation rate is too small to be observable even after applying the most optimistic estimates of the boost factor generated by an enhanced population of microhalos. Reference [6] established a list of requirements that a hypothetical DM particle must satisfy to generate both the observed DM density and a detectable annihilation signal. In this paper, we identify DM candidates in the context of supersymmetry that meet these criteria and demonstrate that the boost to the annihilation rate from an EMDE can bring these hitherto untestable DM candidates squarely within the realm of observation if at least some early forming microhalos survive their accretion into larger microhalos. The existence of these candidates motivates the computationally challenging N-body simulations that are required to conclusively determine the microhalo boost factor and realize these potential constraints on supersymmetric DM.

We focus on supersymmetric bino DM with mass $m_\chi \sim \mathcal{O}(100\text{–}500)$ GeV and with sfermions, gauginos, and Higgsinos decoupled. To obtain boosted annihilation rates that are within the realm of observation by Fermi-LAT, we consider models with an intermediate extended Higgs sector. The pseudoscalar Higgs boson A has mass $m_A \sim \mathcal{O}(m_\chi)$—$\mathcal{O}(1200)$ GeV, and the bino DM annihilates mainly through the s-channel. Spectra with heavy supersymmetry and an intermediate Higgs sector have been studied recently [7]. Apart from the usual reasons to study split supersymmetry, these scenarios are increasingly motivated by bounds on gluinos and charginos coming from the LHC.

These binos exemplify how an EMDE can widen the scope of viable and testable DM models. They have annihilation cross sections that are suppressed by $\mathcal{O}(10^{-3}\text{–}10^{-6})$ compared to the canonical cross section for thermal weakly interacting massive particles and scattering cross sections with atomic nuclei that are typically under the neutrino floor. In standard thermal cosmology, an isolated DM candidate like this overcloses the Universe and its annihilation rate is too small to be constrained by astronomical observations. In the nonthermal cosmology described above, however, such a candidate can generate the observed DM density if its number density is diluted by entropy production during the EMDE. Moreover, its feeble scattering cross section with nuclei ensures that the DM kinetically decouples early enough to preserve the EMDE's enhancement of small-scale inhomogeneity. If the microhalos that form at redshifts greater than $\sim$100 survive within later-forming microhalos, the resulting boost to the annihilation rate brings these isolated DM models within the reach of current observations.

We begin in Sec. II by reviewing how an EMDE affects the relic abundance and kinetic decoupling of dark matter. In Sec. III, we describe the properties of the binos that satisfy the criteria on the kinetic decoupling temperature and the annihilation cross section required to generate the observed DM density during an EMDE and a potentially detectable annihilation signal. We present the results of our scans of this parameter space in Sec. IV and identify DM candidates that generate detectable annihilation signals for different values of the microhalo boost factor. We summarize our findings and discuss the outlook for detecting isolated DM in Sec. V. We use natural units ($\hbar = c = k_B = 1$) in all our expressions.

II. DARK MATTER DURING AN EMDE

During the EMDE, we assume that the energy density of the Universe is dominated by an oscillating scalar field that decays into relativistic particles. The scalar's decay rate Γ_ϕ determines the reheat temperature $T_{\rm RH}$, which is the temperature of the radiation bath when the Universe became radiation dominated (e.g., [2][]),

$$\Gamma_\phi = \sqrt{\frac{8\pi^3 g_*(T_{\rm RH})}{90}}\frac{T_{\rm RH}^2}{m_{\rm Pl}}, \tag{1}$$

where $m_{\rm Pl} = \sqrt{1/G}$ is the Planck mass, and $g_*(T) \equiv \rho_r(T)/[(\pi^2/30)T^4]$ is the number of relativistic degrees of freedom. It is important to note that $T_{\rm RH}$ is not the maximum temperature of the relativistic plasma. On the contrary, the continual decay of the scalar field during the EMDE generates a thermal bath that cools as $T \propto a^{-3/8}$, where a is the scale factor [2]. When the Universe becomes radiation dominated, the plasma begins to cool as $T \propto a^{-1}$, but the temperature remains a monotonically decreasing function of time.

Since $T > T_{\rm RH}$ during the EMDE, it is possible to thermally produce DM even if $m_\chi \gg T_{\rm RH}$. This is the scenario we are interested in: we assume that DM thermally decouples (freezes out) during the EMDE and that there is negligible production of DM from scalar decays. The former assumption requires that the annihilation cross section is large enough to bring DM into thermal equilibrium, failing which it "freezes in," an option we do not consider further because the relevant annihilation cross sections are too small to generate observable signatures [6]. The latter assumption depends on details of the inflaton or modulus sector, and can be realized if the field couples weakly to R-odd particles.

After DM thermally decouples at a temperature T_f, the comoving number density of DM particles remains constant. In contrast, relativistic particles are continuously created by inflaton/moduli decays during the EMDE, so the DM-to-photon ratio is diluted, and the current DM density is suppressed. If DM freezes out after reheating, $\langle\sigma v\rangle \simeq 3 \times 10^{-26}\ {\rm cm^3\ s^{-1}}$ results in the observed DM density ($\Omega_\chi h^2 = 0.12$, where Ω_χ is ρ_χ divided by the critical

density with $H_0 = 100h$ km/s/Mpc [8]), but if $T_f > T_{\rm RH}$ then the resulting DM density is [2,6]

$$\Omega_\chi h^2 \simeq 1.6\times10^{-4}\frac{\sqrt{g_*(T_{\rm RH})}}{g_*(T_f)}\left(\frac{m_\chi/T_f}{15}\right)^4\left(\frac{150}{m_\chi/T_{\rm RH}}\right)^3 \times\left(\frac{3\times10^{-26}\ {\rm cm^3\ s^{-1}}}{\langle\sigma v\rangle}\right). \quad (2)$$

Therefore, $\langle\sigma v\rangle \ll 3\times10^{-26}\ {\rm cm^3\ s^{-1}}$ is required to generate the observed DM relic density during an EMDE, and models that would otherwise overclose the Universe become viable.

After DM thermally decouples, DM is still kept in local kinetic equilibrium by scattering processes with SM particles. At temperatures greater than the kinetic decoupling temperature $T_{\rm kd}$, which is approximately defined as the temperature at which the momentum transfer rate falls below the Hubble expansion rate, DM particles are tightly coupled to the thermal bath, which alters the evolution of the DM density perturbations. Furthermore, the kinetic energy of the DM particles when they decouple determines their comoving free-streaming horizon [9,10]. The average velocity of a dark matter particle at decoupling is $\sim\sqrt{T_{\rm kd}/m_\chi}$. The velocity of a fully decoupled nonrelativistic particle is proportional to a^{-1}, so the comoving free-streaming horizon is

$$\lambda_{\rm fs} = \int_{t_{\rm kd}}^{t_0}\frac{v}{a}{\rm d}t \simeq \sqrt{\frac{T_{\rm kd}}{m_\chi}}a(T_{\rm kd})\int_{a(T_{\rm kd})}^{1}\frac{{\rm d}a}{a^3H(a)}. \quad (3)$$

Perturbations with wavelengths smaller than $\lambda_{\rm fs}$ are erased, which prevents the formation of microhalos if $T_{\rm kd} \lesssim T_{\rm RH}$.

We are interested in kinetic decoupling temperatures that are higher than the reheat temperature so that DM kinetically decouples during the EMDE. Since the expansion rate at a given temperature is faster during the EMDE than during radiation domination, DM decouples at a higher temperature ($T_{\rm kd}$) than it would have in a purely radiation-dominated era ($T_{\rm kd,RD}$). If the velocity-averaged elastic scattering cross section of DM ($\langle\sigma_{\rm el}v\rangle$) is proportional to T^2, the expansion rate during the EMDE implies that DM decouples when $T_{\rm kd} \sim T_{\rm kd,RD}^2/T_{\rm RH}$ [10]; the exact dependence is given by [6],

$$T_{\rm kd} = \left[\frac{g_*(T_{\rm kd})^2}{g_*(T_{\rm kd,RD})g_*(T_{\rm RH})}\right]^{1/4}\sqrt{\frac{5}{2}}\frac{T_{\rm kd,RD}^2}{T_{\rm RH}}. \quad (4)$$

This relationship between $T_{\rm kd}$ and $T_{\rm kd,RD}$ assumes that no new scattering channels open up at temperatures higher than $T_{\rm kd,RD}$ and lower than $T_{\rm kd}$ so that $\langle\sigma_{\rm el}v\rangle \propto T^2$ between these temperatures. It makes no other assumptions regarding the precise definition of the momentum transfer rate and can accommodate any definition that is proportional to $\langle\sigma_{\rm el}v\rangle n_\ell(T/m_\chi)$, where $n_\ell \propto T^3$ is the number density of relativistic particles that elastically scatter DM.

III. ISOLATED BINOS

Since our primary example is bino DM in supersymmetric models, we give some details about its interactions with SM fermions, which determine its scattering cross section and decoupling temperature. The scattering cross section of bino DM with SM particles has been studied in detail by [11] and implemented in DarkSUSY [12]. The scattering cross section between neutralinos and SM fermions is mediated by the exchange of sfermions in the s- and u-channels, and Z bosons as well as light and heavy scalar Higgs exchanges in the t-channel. We study each contribution in turn, starting with the s- and u-channels.

The coupling of binos to sfermions ($\tilde f$) and SM fermions (f) can be written as

$$\mathcal{L} = -\sqrt{2}g\bar f\{\alpha\tilde f_L\mathcal{P}_R - \beta\tilde f_R\mathcal{P}_L\}\chi + {\rm H.c.} \quad (5)$$

where $\alpha = \frac{Y_f}{2}\tan\theta_W$ and $\beta = Q_f\tan\theta_W$, with g, Y_f, and Q_f being the electroweak coupling constant, weak hypercharge, and the electric charge of the fermion, respectively. We consider fermion energies ω in the regime of low momentum transfer, with $\omega \ll m_\chi$, $t\to0$, and $s \to m_\chi^2 + 2m_\chi\omega + m_\ell^2$, where s and t are the usual Mandelstam variables. Note that the approximation $v\sim1$ for the Moeller velocity is very good in this case. The elastic scattering rate for $\chi+\ell\to\chi+\ell$, $\Gamma_{\rm el} = \sum_\ell\langle v\sigma_{\rm el}(\omega_\ell)\rangle(T)n_\ell(T)$ is then given by

$$\Gamma_{\rm el} = \frac{288}{\pi}\sum_L(\alpha^4+\beta^4)\left(\frac{G_{\rm F}M_W^2}{m_{\tilde\ell}^2 - m_\chi^2}\right)^2T^2n_\ell, \quad (6)$$

where n_ℓ denotes the number density of leptons ℓ, $m_{\tilde\ell}$ denotes the slepton mass, and the sum is over SM leptons. The momentum transfer rate can be determined from the number of scatterings required to change the momentum of a DM particle significantly: $\Gamma_{\rm mt} \simeq \sqrt{3/2}(T/m_\chi)\Gamma_{\rm el}$ [11]. The kinetic decoupling temperature is defined by requiring $\Gamma_{\rm mt} \simeq H$. For sleptons in the 10–100 TeV mass range, one can obtain $T_{\rm kd,RD}$ values as high as $\mathcal{O}(1$–$5)$ GeV.

The t-channel scattering diagrams are facilitated by the bino-Higgsino mixture of the DM candidate χ. This mixture is usually parametrized as

$$\chi = N_{11}\tilde B + N_{12}\tilde W + N_{13}\tilde H_d + N_{14}\tilde H_u \quad (7)$$

where N_{11}, N_{12}, N_{13}, and N_{14} denote projections of χ along the bino ($\tilde B$), wino ($\tilde W$), and Higgsino ($\tilde H_d$ and $\tilde H_u$) directions, respectively. Since the DM is primarily bino, one has $N_{11}\sim1$, while

$$\frac{N_{13}}{N_{11}} \sim \frac{m_Z \sin\theta_W}{\mu} \sin\beta$$
$$\frac{N_{14}}{N_{11}} \sim \frac{m_Z \sin\theta_W}{\mu} \cos\beta. \quad (8)$$

In the above, μ denotes the Higgsino mass parameter while $\tan\beta$ denotes the ratio of the Higgs vacuum expectation values, and is taken to be $\mathcal{O}(10)$. The Weinberg angle is denoted by θ_W. We have displayed simplified expressions in the limit of $\mu \gg m_\chi$.

In the limit of relativistic SM fermions, we keep contributions to the scattering amplitude that are leading order in (m_ℓ/ω), where m_ℓ is the mass of a SM fermion and ω its energy. Moreover, we keep contributions that are leading order in (ω/m_χ). The scattering amplitude from t-channel exchange can then be obtained as [11]

$$\mathcal{M}_t^2 \sim 8\left(\frac{\omega}{m_\chi}\right)^2\left(\frac{m_\chi}{m_Z}\right)^4 g_{Z\chi\chi,L}^2 (g_{Z\ell\ell,L}^2 + g_{Z\ell\ell,R}^2), \quad (9)$$

where $g_{Z\chi\chi}$ and $g_{Z\ell\ell}$ denote the coupling of Z to DM and a SM fermion ℓ, respectively. The subscripts L and R denote left- and right-handed projections, respectively. In terms of the bino-Higgsino content of the DM χ, the coupling $g_{Z\chi\chi}$ is given by [13,14]

$$g_{Z\chi\chi} = 2^{1/4} G_F^{1/2} M_W \frac{1}{\cos\theta_W}(N_{13}^2 + N_{14}^2)$$
$$\sim 2^{1/4} G_F^{1/2} M_W \frac{\sin^2\theta_W}{\cos\theta_W}\left(\frac{m_Z}{\mu}\right)^2. \quad (10)$$

We note that terms coming from the exchange of light and heavy Higgs bosons come at the next order in (m_ℓ/ω) in $\mathcal{M}_t^2$.

The scattering amplitude can be used to obtain the elastic scattering following a calculation that is very similar to the s-channel case. One obtains

$$\Gamma_{\rm el} \sim \left(\frac{G_F M_W^2}{\mu^2}\right)^2 T^2 n_\ell. \quad (11)$$

Similar to the s-channel case, the Higgsino mass parameter μ should also be kept in the 10–100 TeV range to obtain $T_{\rm kd,RD}$ in the range of $\mathcal{O}(1$–$5)$ GeV.

We note that the computations in this section are meant to clarify the general features of the spectrum; for actual numerical calculations, the exact expressions are used. Additionally, we use DarkSUSY to compute the kinetic decoupling temperature in a radiation-dominated Universe. DarkSUSY defines $T_{\rm kd,RD}$ as the instantaneous decoupling temperature that predicts the asymptotic late-time evolution of the DM temperature [15]. This definition of $T_{\rm kd,RD}$ differs from the momentum-rate definition by a factor of order unity [16]. As mentioned earlier, however, Eq. (4) for the kinetic decoupling temperature during an EMDE applies to any definition of $T_{\rm kd,RD}$ if $\langle\sigma_{\rm el} v\rangle \propto T^2$.

In summary, for heavy s-channel mediators (heavy sleptons) or suppressed coupling of DM to t-channel mediators [caused by large μ or heavy Higgsinos, and consequently small Higgsino component in the DM candidate, following Eq. (8)], one has small scattering rates of the DM, and hence relatively large kinetic decoupling temperatures. Moreover, the same features of the spectrum lead to a reduced annihilation rate (which necessitates the EMDE to obtain the observed relic density), as well as reduced scattering rates off of nuclei, and hence reduced signal rates at direct detection experiments. It is in the above senses that these DM candidates are isolated.

IV. RESULTS

Obtaining observable enhancement of the DM annihilation rate hinges on two requirements: (i) the EMDE sufficiently enhances small-scale perturbations (the halo is clumpy enough) to greatly boost the DM annihilation rate, and (ii) the annihilation cross section is large enough that the boosted rate falls within the observable range of current and future experiments. To quantify these two requirements, we define the quantities $k_{\rm kd}$ and $k_{\rm RH}$, which are the wave numbers of the modes that enter the horizon at $T = T_{\rm kd}$ and $T = T_{\rm RH}$, respectively, as well as $k_{\rm fs} = \lambda_{\rm fs}^{-1}$ and $k_{\rm cut} = \min(k_{\rm kd}, k_{\rm fs})$. We assume that perturbations are exponentially suppressed for $k > k_{\rm cut}$. However, we note that while such a suppression occurs when dark matter kinetically decouples during radiation domination [9], it has not been proven that this behavior extends to decoupling during an EMDE. In particular, since perturbations in the radiation density grow during an EMDE [4,5], momentum exchange between the dark matter particles and relativistic leptons does not generate dark acoustic oscillations and may not completely prevent the growth of matter perturbations with $k > k_{\rm kd}$.

The Press-Schechter formalism [17] requires that the rms density perturbation exceed a critical value for the formation of microhalos. Therefore, the microhalo population depends strongly on the ratio $k_{\rm cut}/k_{\rm RH}$, which determines the masses of the smallest microhalos and the timing of their formation. By studying the dependence of the Press-Schechter differential bound fraction on $k_{\rm cut}/k_{\rm RH}$, Ref. [6] found that the EMDE dramatically increases the microhalo population if $k_{\rm cut}/k_{\rm RH} \geq 10$, which translates to

$$T_{\rm kd,RD}/T_{\rm RH} \geq 2 \quad (12)$$

for values of $T_{\rm RH}$ and m_χ in the range we are interested in. This is the first requirement on our supersymmetric parameter space, and can be recast in several other ways. From the relationship between $T_{\rm kd,RD}$ and $T_{\rm kd}$, this translates approximately to $T_{\rm kd}/T_{\rm RH} > 2\sqrt{10}$, which, since we

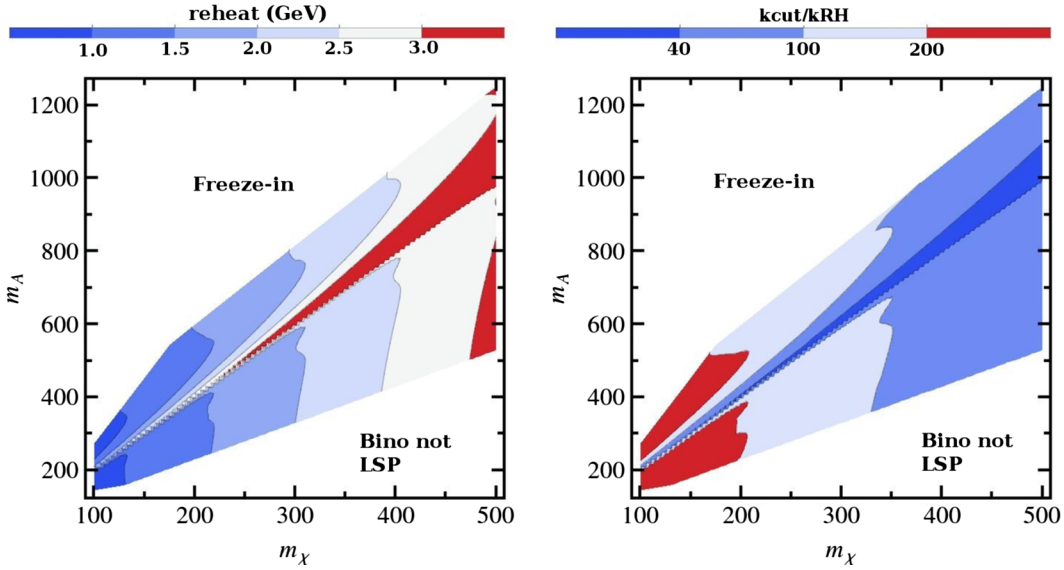

FIG. 1. The distribution of reheat temperatures (left panel) and $k_{\rm cut}/k_{\rm RH}$ (right panel) on the (m_χ, m_A) plane. Here $k_{\rm cut} = \min(k_{\rm kd}, k_{\rm fs})$. All points satisfy the relic density constraint. Fixed values of sfermion masses $m_{\tilde{f}} = 60$ TeV, Higgsinos $\mu = 150$ TeV, and $\tan\beta = 8$ are assumed. Masses on the horizontal and vertical axes are in GeV.

require that DM freezes out prior to kinetic decoupling, implies that $T_f/T_{\rm RH} > 2\sqrt{10}$. Since the freeze-out temperature is approximately given as $T_f \sim m_\chi/10$, it turns out that one typically needs $m_\chi/T_{\rm RH} > 100$ for Eq. (12) to hold. Given this range of $m_\chi/T_{\rm RH}$, using Eq. (2), one obtains that the annihilation cross section is bounded from above. This upper bound is most conveniently expressed as $\frac{\langle\sigma v\rangle}{m_\chi^2} \lesssim 10^{-16}$ GeV^{-4}, as can be checked by the exact numerical calculations. Consequently, we are most interested in particles with

$$10^{-20}\ \text{GeV}^{-4} \lesssim \frac{\langle\sigma v\rangle}{m_\chi^2} \lesssim 10^{-16}\ \text{GeV}^{-4}: \qquad (13)$$

the upper bound ensures that the EMDE enhances the abundance of microhalos, while the lower bound is required to bring the final boosted annihilation rate within the realm of current observations for at least some estimates of the boost factor.

We scan the parameter space of bino DM in the minimal supersymmetric standard model, keeping the constraints of Eqs. (12) and (13) in mind. For each value of $\langle\sigma v\rangle$ and m_χ, the reheat temperature $T_{\rm RH}$ is chosen such that the relic density constraint $\Omega_\chi h^2 = 0.12$ is satisfied from Eq. (2). In order to satisfy Eq. (12), all sfermions are kept at $\sim\mathcal{O}(60)$ TeV, and charged and neutral Higgsinos at $\mathcal{O}(100)$ TeV. The winos and the gluino are kept at a few TeV and we choose $\tan\beta = 8$. The results of the scan are displayed in Fig. 1.

For each set of parameters, we numerically determined the present-day dark matter density to confirm that all models in the scan satisfy the relic density constraint. We note that Eq. (2) for the relic density depends on the reheat temperature as $\Omega_\chi h^2 \propto (T_{\rm RH}/m_\chi)^3$. Consequently, larger values of m_χ require higher reheat temperatures to keep $\Omega_\chi h^2 = 0.12$. The relic density is also proportional to $\langle\sigma v\rangle^{-1}$, which implies that the enhancement of $\langle\sigma v\rangle$ when $m_A \simeq 2m_\chi$ suppresses the relic density, and a larger value of $T_{\rm RH}/m_\chi$ is required to compensate. Both of these features are visible in the left panel of Fig. 1. For the range of DM masses we consider, $T_{\rm RH}$ is required to be in the range of 1 to a few GeV. This range of reheat temperatures is in fact naturally obtained in explicit models of the modulus sector that are responsible for the EMDE [18,19].

After obtaining $T_{\rm kd,RD}$ from DarkSUSY, we calculate $T_{\rm kd}$ and $\lambda_{\rm fs}$, which enables us to find $k_{\rm cut}/k_{\rm RH}$. The corridor along which the pseudoscalar resonance is most effective corresponds to the highest $T_{\rm RH}$ and lowest $k_{\rm cut}/k_{\rm RH}$ values, as expected. The left panel shows that most models in the scan satisfy $m_\chi/T_{\rm RH} > 100$.

We now turn to the boost-factor calculation, which offers hope of constraining these models in spite of their small annihilation cross sections. Using the Press-Schechter formalism to predict the microhalo abundance, Ref. [6] estimated the resulting boost to the annihilation rate by assuming that all microhalos present at a certain redshift have Navarro-Frenk-White (NFW) profiles and that the central regions of these microhalos survive to the present day.[1] All the microhalos were assumed to have the same

[1]While phase-density conservation and DM annihilations are expected to generate deviations from the NFW profile, the resulting constant-density cores are too small to significantly alter the annihilation rate within the microhalos [6].

concentration, $c = 2$, which is the lowest concentration seen in simulations of microhalo formation [20,21]. This assumption effectively implies that all the microhalos are newly formed at the redshift z_f at which the microhalo population is evaluated and therefore provides a conservative estimate of the boost factor. The calculated boost factors are highly sensitive to the choice of z_f. The boost factor is proportional the fraction of dark matter that is bound in EMDE-enhanced microhalos at z_f. It is also proportional to the matter density at that redshift because earlier-forming microhalos have denser central regions.[2]

The fraction of matter that is contained in microhalos is largely insensitive to the reheat temperature but highly sensitive to the ratio $k_{\rm cut}/k_{\rm RH}$, which determines the redshift at which the first microhalos form [6]. If $k_{\rm cut}/k_{\rm RH} = 10$, 30% of the dark matter is bound into microhalos at a redshift of 50 and 5% is bound at a redshift of 100. This is a significant enhancement of the microhalo abundance; in the absence of an EMDE, less than 4% of the dark matter is contained in halos at a redshift of 50. The effect of the EMDE is even larger for larger values of $k_{\rm cut}/k_{\rm RH}$. If $k_{\rm cut}/k_{\rm RH} = 20$, then 5% of the dark matter is bound into microhalos at a redshift of 400, and the bound fraction increases to 75% at a redshift of 50. If $k_{\rm cut}/k_{\rm RH} = 40$, then 60% of the dark matter is bound into microhalos at a redshift of 400, and this bound fraction increases to 90% at a redshift of 50.

The right panel of Fig. 1 indicates that the isolated binos we consider can have even larger values of $k_{\rm cut}/k_{\rm RH}$, so we have extended the Ref. [6] analysis to $k_{\rm cut}/k_{\rm RH} = 60$ and $k_{\rm cut}/k_{\rm RH} = 80$. For these values of $k_{\rm cut}/k_{\rm RH}$, microhalos are prevalent at even higher redshifts, with bound fractions of 75% and 86%, respectively, at a redshift of 600 and above 94% at a redshift of 50. Microhalos are also common at redshifts greater than 600 in these scenarios, but our calculations assume that the Universe is matter dominated and should not be extended beyond $z \simeq 600$.

This abundance of microhalos at redshifts greater than 100 stands in sharp contrast to standard expectations: in the absence of an EMDE, the Press-Schechter formalism predicts that 0.02% of the dark matter is bound into halos with masses greater than $10^{-20} M_\odot$ at $z = 100$. Therefore, the formation time of the first microhalos is rather insensitive to the minimum halo mass, as even the smallest microhalos are very rare before $z = 100$. All halos form at roughly the same time in these cosmologies because the dimensionless matter power spectrum depends only logarithmically on k on small scales. In contrast, an EMDE makes the dimensionless matter power spectrum proportional to $k^{(n_s+3)}$ for $k > k_{\rm RH}$, where $n_s \simeq 1$ is the scalar spectral index, which allows smaller halos to form long before larger halos. Therefore, increasing $k_{\rm cut}/k_{\rm RH}$ significantly increases the redshift at which microhalos are common in EMDE scenarios and dramatically increases the boost factor if these dense early forming microhalos survive.

The appropriate choice of z_f when calculating the boost factor depends on the outcome of microhalo-microhalo mergers: do the microhalos present at $z \gtrsim 400$ survive as subhalos of the microhalos that contain most of the dark matter at $z \simeq 50$? If they survive, then we should use $z_f = 400$ to estimate the boost factor B, and for the nearest dwarf spheroidals (dSphs), $1 + B \simeq 20,000$ for $k_{\rm cut}/k_{\rm RH} \simeq 20$, 200,000 for $k_{\rm cut}/k_{\rm RH} \simeq 40$, and 300,000 for $60 \lesssim k_{\rm cut}/k_{\rm RH} \lesssim 80$ [6]. If the microhalos present at $z = 600$ also survive as subhalos, then it is possible to obtain boost factors larger than 800,000 for $k_{\rm cut}/k_{\rm RH} \gtrsim 60$.

However, if the dense central regions of the first microhalos do not survive as subhalos of later-forming microhalos, then we should take $z_f = 50$, as the EMDE-enhanced microhalo abundance peaks at this redshift.[3] As mentioned earlier, our assumption that all microhalos have a concentration of 2 at z_f implies that the boost factor is proportional to the matter density at z_f. Therefore, if the bound fraction is $\mathcal{O}(1)$ at $z_f = 400$, as is the case for $k_{\rm cut}/k_{\rm RH} \gtrsim 40$, setting $z_f = 50$ instead of $z_f = 400$ reduces the boost factor by roughly a factor of $(51/401)^3 = 0.002$, with some adjustment due to variation in the bound fraction between the two redshifts. As a result, taking $z_f = 50$ reduces the dSph boost factors to between 200 and 700 for $10 \lesssim k_{\rm cut}/k_{\rm RH} \lesssim 80$ [6]. These boost factors are surely underestimated, however, because their derivation assumes that the microhalos present at a redshift of 50 have no substructure and neglects the fact many of these microhalos formed at much higher redshifts and therefore have concentrations greater than 2.

Clearly, numerical simulations of microhalo formation in EMDE scenarios are required to determine the fate of the first generation of microhalos and to robustly compute the boost factor generated by an EMDE. In the absence of such simulations, we are forced to adopt a wide range of possible boost factors for different values of $k_{\rm cut}/k_{\rm RH}$, as shown in Table I. We consider boost factors calculated using three values of z_f. In the most pessimistic scenario, we assume that all early forming microhalos are destroyed and we take $z_f = 50$. In the most optimistic scenario, we choose z_f so that the boost factor is maximized, i.e., the largest redshift

[2]The dependence of the boost factor on the matter density implies that choosing a higher concentration for the microhalos has the same effect on the boost factor as increasing z_f. For example, choosing $c = 5$ instead of $c = 2$ has the same effect increasing $(1 + z_f)$ by a factor of 1.44: in both cases, the boost factor increases by a factor of 3 [6].

[3]For all values of $k_{\rm cut}/k_{\rm RH}$, the abundance of EMDE-enhanced microhalos decreases at redshifts below 25 as they are absorbed into larger halos. However, the dense cores of the EMDE-enhanced microhalos are expected to survive within these much-later forming halos [6].

TABLE I. Fiducial values of the EMDE boost factor for the nearest dSphs. The minimum values were based on the microhalo population at a redshift of 50 with no substructure and a universal halo concentration of 2. The maximum values were based on the microhalo population at a redshift that maximizes the boost factor, up to $z = 400$ for $k_{\rm cut}/k_{\rm RH} < 60$ and $z = 600$ for $k_{\rm cut}/k_{\rm RH} \geq 60$. Finally, the intermediate values are based on the microhalo population at an intermediate redshift: $z = 50$ for $k_{\rm cut}/k_{\rm RH} < 20$, $z = 100$ for $20 \leq k_{\rm cut}/k_{\rm RH} < 40$, and $z = 200$ for $k_{\rm cut}/k_{\rm RH} \geq 40$.

	Minimum	Intermediate	Maximum
$k_{\rm cut}/k_{\rm RH} < 10$	1	1	1
$10 \leq k_{\rm cut}/k_{\rm RH} < 20$	200	200	300
$20 \leq k_{\rm cut}/k_{\rm RH} < 40$	500	3000	20,000
$40 \leq k_{\rm cut}/k_{\rm RH} < 60$	600	30 000	200 000
$60 \leq k_{\rm cut}/k_{\rm RH} < 80$	650	40 000	800 000
$80 < k_{\rm cut}/k_{\rm RH}$	700	40 000	1 000 000

with a significant bound fraction. We note that even this model may underestimate the boost factor, however, because it neglects all structure formation at redshifts lower than z_f. Finally, we consider a model that assumes that the earliest microhalos are destroyed, but those that form at $z \lesssim 200$ survive. In addition to providing an intermediate case, this model exemplifies the smallest boost factors that generate detectable annihilation rates within dSphs.

As previously mentioned, the precise relationship between the decoupling temperature and the cutoff scale may differ from the relation established in Refs. [9,15] when dark matter decouples during an EMDE. To mitigate the effects of this uncertainty, we use the same boost factor for a range of $k_{\rm cut}/k_{\rm RH}$ values. For each interval listed in Table I, the given boost factor was computed assuming the smallest value of $k_{\rm cut}/k_{\rm RH}$ within that range. We also note that once the bound fraction of dark matter approaches unity at z_f, further increases in $k_{\rm cut}/k_{\rm RH}$ do not significantly change the boost factor. Consequently, the boost factor is rather insensitive to changes in $k_{\rm cut}$ if $k_{\rm cut}/k_{\rm RH} > 40$ in the intermediate case and $k_{\rm cut}/k_{\rm RH} > 60$ in the maximum case. The right panel of Fig. 1 shows that only a very narrow region of parameter space along the pseudoscalar resonance has $k_{\rm cut}/k_{\rm RH} \lesssim 40$, so we expect that our results would not be significantly altered by the changes in the definition of $k_{\rm cut}$ that could result from an improved understanding of kinetic decoupling during an EMDE.

Unfortunately, it is difficult to directly compare the boosted annihilation rate to constraints from Fermi-LAT's observations of dSphs [22]. Although these constraints are dominated by the contribution from the nearest dSphs, they are enhanced by limits on DM annihilation within more massive dSphs, which would have even larger boost factors [6]. Furthermore, these constraints are derived under the assumption the DM annihilation rate is proportional to the square of the DM density within the dSph, which implies that any potential DM signal originates from the dSph's central region. In EMDE scenarios, however, annihilations within microhalos overshadow the contribution from the smooth density profile of the dSph. Instead, the signal profile tracks the number density of microhalos, which is expected to follow the average DM density outside

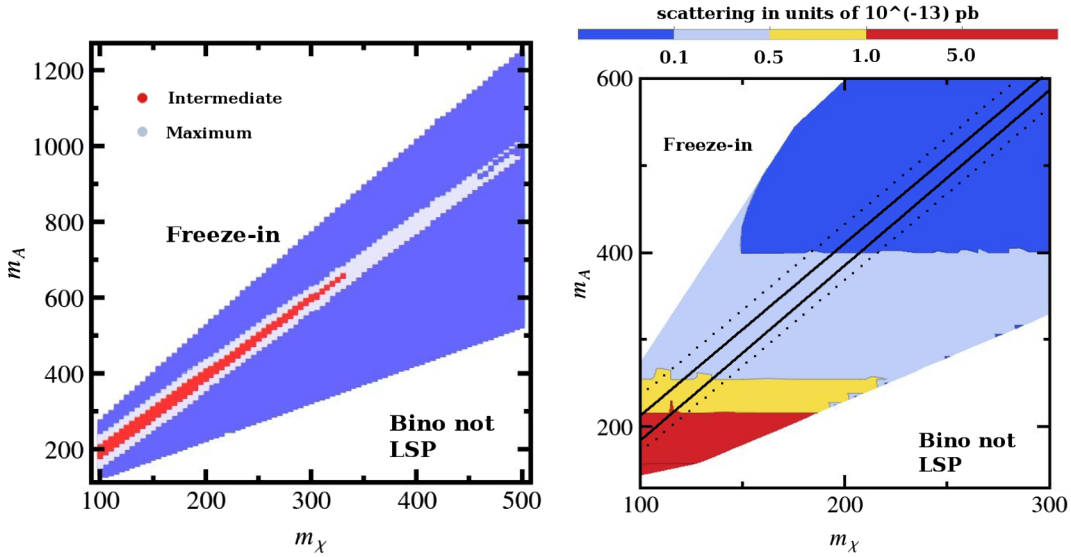

FIG. 2. Models constrained by six-year Pass 8 Fermi-LAT dwarf galaxy data (left panel) and the corresponding scattering cross sections off nuclei in units of 10^{-13} pb (right panel). Left panel: The red (light blue) region is being probed by current observations using intermediate (maximum) estimates of the EMDE boost factor (see Table I). Right panel: Regions that are not red are mostly under the neutrino floor. The solid (dashed) black line shows the region corresponding to the red (light blue) of the left panel. Masses on the horizontal and vertical axes are in GeV.

of the dSph's innermost 40 pc, where microhalos are most likely destroyed by tidal forces [6]. Fermi-LAT's observation window is large enough to include most of the mass in the nearest dSphs (and therefore most of their microhalos), but it is uncertain how changing the expected DM emission profile would alter their constraints on the DM annihilation rate. However, in light of the extreme uncertainty present in the boost factor, we ignore these issues and consider a particle accessible to Fermi-LAT if $(1+B)\langle\sigma v\rangle$ exceeds the Fermi-LAT collaboration's six-year Pass 8 limits on the DM annihilation cross section from observations of dSphs [22].

The left panel of Fig. 2 shows the regions of the parameter space that are accessible to Fermi-LAT for the different boost-factor models given in Table I. The models marked in red (light blue) indicate those constrained by six-year Pass 8 Fermi-LAT dwarf galaxy observations [22] after imposing intermediate (maximum) boost factors from Table I. We note that annihilation cross sections in the zero velocity limit (present Universe) were taken when applying the boost factors and imposing constraints. Although the s-channel exchange of the pseudoscalar Higgs boson leads to a velocity-independent annihilation cross section, velocity dependence nevertheless comes from the well-known effect of resonance broadening [23]. The location of the pseudoscalar resonance region is velocity dependent and thus shifts in the current Universe, compared to the freeze-out era.

The pseudoscalar resonance width depends on $\tan\beta$, and in the low $\tan\beta \sim 3$ and high $\tan\beta \sim 50$ regions, the width is quite large, $\Gamma \sim 0.05 m_A$ [24]. This allows one to constrain a relatively broad region of parameter space away from the line $m_A = 2m_\chi$, as shown in the left panel of Fig. 2. Beyond the light blue region where the maximum boost factors are applied, the annihilation cross section is too feeble to be constrained by Fermi-LAT, even after incorporating the maximal boost factors.

The right panel shows the corresponding spin-independent scattering cross sections relevant for direct detection; regions that are not red are under the neutrino floor. The solid (dashed) black line shows the region corresponding to the red (light blue) of the left panel. As discussed previously, the isolated nature of the DM renders scattering cross sections, and hence signal rates at direct detection experiments, exceedingly small.

V. SUMMARY AND OUTLOOK

The results of this paper are of interest from the perspective of astrophysics as well as particle physics. We have identified realistic examples where the physics of microhalo formation during an EMDE plays a decisive role in the detectability of DM candidates. The conditions that a DM candidate has to satisfy are encapsulated in Eqs. (12) and (13). We have shown that even the most garden variety DM candidate, the bino of supersymmetry, can satisfy these conditions in certain classes of supersymmetric spectra.

Even broader lessons can be taken away on the particle physics side. In standard thermal cosmologies, DM candidates that interact extremely feebly with SM particles neither satisfy the relic density nor hold out any hope of direct or indirect detection. For example, candidates that satisfy Eq. (12) have scattering rates with SM particles that are feeble, leading to a large kinetic decoupling temperature and small detection rates at direct detection experiments (typically below the neutrino background). Moreover, the same feeble interactions lead to Eq. (13), a suppressed annihilation cross section compared with the canonical value.

We have shown that these DM candidates are not ruled out by their relic abundance, nor are they necessarily undetectable. An EMDE can dilute the DM relic density so that even candidates satisfying Eq. (13) can generate the observed relic density. The relatively high kinetic decoupling temperature, following from Eq. (12), can lead to the formation of microhalos that boost the feeble annihilation rate and may bring some parts of the parameter space within the range of detection by Fermi-LAT. The bino model we consider can be thought of as an example of this broader field of DM candidates.

The existence of these DM candidates motivates further study of the effect an EMDE has on the DM annihilation rate within galactic halos. An EMDE enhances small-scale structure: the Press-Schechter formalism predicts that most of the dark matter is bound into microhalos at high redshift ($z \gtrsim 100$). These microhalos merge to form larger microhalos at $z \simeq 50$ that then act as the building blocks of subsequent structure formation. Analytical estimates of the resulting boost to the annihilation rate of these particles within nearby dSphs range from a factor of 100 to a factor of 10^6, depending on the fate of the early generations of microhalos. We have shown that a boost factor $\gtrsim 10^4$ is required to exceed the bounds on the DM annihilation rate established by Fermi-LAT observations. This boost factor can be obtained if the microhalos present at $z \simeq 100$ survive as subhalos within later-forming microhalos. N-body simulations of microhalo formation in EMDE cosmologies are required to determine if this boost factor is realized, which would allow Fermi-LAT to rule out these otherwise undetectable binos as DM candidates. On the particle physics side, it would be interesting to explore, in greater detail, supersymmetric spectra with an intermediate extended Higgs sector in light of these potential observational constraints.

ACKNOWLEDGMENTS

We thank JiJi Fan and Tim Tait for useful comments on an earlier draft of this paper. We also thank the referee for many questions and comments that have improved the quality of this paper. A. E. is supported by NSF Grant

No. PHY-1417446. K. S. and S. W. are supported by NASA Astrophysics Theory Grant No. NNH12ZDA001N. S. W. is also supported by DOE Award No. DE-FG02-85ER40237.

Note added.—Recently, the referee raised an interesting question: does the formation of primordial black holes (PBHs) place restrictions on the EMDE? Indeed, it is the enhanced growth of density perturbations during the EMDE that leads to the interesting dark matter phenomenology discussed in this paper, and it is reasonable to suspect that this increased inhomogeneity could also generate PBHs. The question of PBH constraints was examined by one of the authors and his collaborators in Ref. [25]. There it was found that the strongest constraints arise from limits on the abundance of PBHs with masses around 10^{15} grams: for these PBHs, Hawking radiation produces gamma rays that would be observable by Fermi-LAT and would leave an imprint on the cosmic microwave background. In Ref. [25] it was shown that these bounds on the abundance of PBHs can only be violated if the primordial power spectrum generated during inflation has a blue tilt. Moreover, an EMDE actually weakens the PBH constraints on the scalar spectral index n_s because the formation of PBHs from increasing inhomogeneity during the EMDE does not compensate for the fact that the relative contribution of PBHs to the total density of the Universe remains constant during the EMDE instead of increasing as it does during radiation domination. Whereas PBHs rule out $n_s \gtrsim 1.1$ in the absence of an EMDE, n_s can be as large as 1.4 if there was an EMDE that ended just before BBN. Therefore, the detection of an extremely blue primordial spectrum on small scales would place an upper bound on the reheat temperature. However, in this paper we have assumed a red primordial power spectrum ($n_s = 0.96$ with no running), and the results of Ref. [25] imply that PBHs provide no constraint on the EMDE in this case.

[1] G. Kane, K. Sinha, and S. Watson, Int. J. Mod. Phys. D **24**, 1530022 (2015).
[2] G. F. Giudice, E. W. Kolb, and A. Riotto, Phys. Rev. D **64**, 023508 (2001).
[3] G. B. Gelmini and P. Gondolo, Phys. Rev. D **74**, 023510 (2006); T. Moroi and L. Randall, Nucl. Phys. **B570**, 455 (2000); B. S. Acharya, P. Kumar, K. Bobkov, G. Kane, J. Shao, and S. Watson, J. High Energy Phys. 06 (2008) 064; P. Grajek, G. Kane, D. Phalen, A. Pierce, and S. Watson, Phys. Rev. D **79**, 043506 (2009); B. Dutta, L. Leblond, and K. Sinha, Phys. Rev. D **80**, 035014 (2009).
[4] A. L. Erickcek and K. Sigurdson, Phys. Rev. D **84**, 083503 (2011).
[5] J. Fan, O. Ozsoy, and S. Watson, Phys. Rev. D **90**, 043536 (2014).
[6] A. L. Erickcek, Phys. Rev. D **92**, 103505 (2015).
[7] G. Lee and C. E. M. Wagner, Phys. Rev. D **92**, 075032 (2015); B. Li and C. E. M. Wagner, Phys. Rev. D **91**, 095019 (2015); E. Bagnaschi, G. F. Giudice, P. Slavich, and A. Strumia, J. High Energy Phys. 09 (2014) 092; A. Anandakrishnan, B. Shakya, and K. Sinha, Phys. Rev. D **91**, 035029 (2015).
[8] P. A. R. Ade *et al.* (Planck Collaboration), arXiv: 1502.01589.
[9] E. Bertschinger, Phys. Rev. D **74**, 063509 (2006).
[10] G. B. Gelmini and P. Gondolo, J. Cosmol. Astropart. Phys. 10 (2008) 002.
[11] S. Hofmann, D. J. Schwarz, and H. Stoecker, Phys. Rev. D **64**, 083507 (2001); T. Bringmann and S. Hofmann, J. Cosmol. Astropart. Phys. 04 (2007) 016; S. Profumo, K. Sigurdson, and M. Kamionkowski, Phys. Rev. Lett. **97**, 031301 (2006).
[12] P. Gondolo, J. Edsjo, P. Ullio, L. Bergstrom, M. Schelke, and E. A. Baltz, J. Cosmol. Astropart. Phys. 07 (2004) 008.
[13] J. Edsjo, arXiv:hep-ph/9704384.
[14] J. Edsjo and P. Gondolo, Phys. Rev. D **56**, 1879 (1997).
[15] T. Bringmann, New J. Phys. **11**, 105027 (2009).
[16] T. Bringmann and S. Hofmann, J. Cosmol. Astropart. Phys. 04 (2007) 016; 03 (2016) E02.
[17] W. H. Press and P. Schechter, Astrophys. J. **187**, 425 (1974).
[18] R. Allahverdi, M. Cicoli, B. Dutta, and K. Sinha, Phys. Rev. D **88**, 095015 (2013).
[19] R. Allahverdi, M. Cicoli, B. Dutta, and K. Sinha, J. Cosmol. Astropart. Phys. 10 (2014) 002.
[20] D. Anderhalden and J. Diemand, J. Cosmol. Astropart. Phys. 04 (2013) 009; 08 (2013) E02.
[21] T. Ishiyama, Astrophys. J. **788**, 27 (2014).
[22] M. Ackermann *et al.* (Fermi-LAT Collaboration), Phys. Rev. Lett. **115**, 231301 (2015).
[23] K. Griest and D. Seckel, Phys. Rev. D **43**, 3191 (1991).
[24] A. Djouadi, L. Maiani, A. Polosa, J. Quevillon, and V. Riquer, J. High Energy Phys. 06 (2015) 168.
[25] J. Georg, G. Sengor, and S. Watson, Phys. Rev. D **93**, 123523 (2016).